Eur. Phys. J. Plus (2014) **129**: 276
DOI 10.1140/epjp/i2014-14276-x

THE EUROPEAN PHYSICAL JOURNAL PLUS

Regular Article

The effect of the thickness ratio of magnetic layers on the microstructure and magnetic properties of $(CoCrPt)_{97.5}Nb_{2.5}/Co_{75}Cr_{13}Pt_{12}/Cr$ thin films

E. Jafari-Khamse[1], M. Almasi-Kashi[1,2,a], A. Ramazani[1,2], and H. Almasi-Kashi[3]

[1] Department of physics, University of Kashan, Kashan, Iran
[2] Institute of Nanoscience and Nanotechnology, University of Kashan, Kashan, Iran
[3] Department of ECE, University of Tehran, Tehran, Iran

Received: 25 November 2014
Published online: 24 December 2014 – © Società Italiana di Fisica / Springer-Verlag 2014

Abstract. A $Co_{75}Cr_{13}Pt_{12}$ intermediate magnetic layer was deposited between the $(CoCrPt)_{97.5}Nb_{2.5}$ upper magnetic layer and chromium underlayer by the magnetron sputtering technique. The effect of the thickness ratio of two magnetic layers and post-annealing treatment on the microstructure and magnetic properties of the films were investigated. The magnetic characteristics of the films were obtained by magnetic force microscopy, hysteresis loops and switching field distribution curves. Although annealing had no significant effect on the layer roughness, it rotated the easy axis of the magnetic layer towards the film plane, thereby enhanced the coercivity. The results showed an impressive effect of the magnetic intermediate layer thickness and post-annealing on the improving of coercivity through isolation of the magnetic grains. Formation of a non-magnetic halo around the magnetic grains reduced the inter-granular magnetostatic interaction.

1 Introduction

The key requirements to achieve ultra-high density magnetic recording are small grain size, preferred crystallographic orientation, high coercivity, high magnetic squareness (ratio of remanent to saturation magnetizations), low remanence-thickness product and low inter-granular coupling through magnetic grain isolation [1,2]. CoCr-based alloys are the best candidates for this purpose because of their strong magnetic anisotropy and low media noise. It is correlated with decoupling of the magnetostatic interaction between the magnetically isolated grains which is compositionally segregated at the grain boundaries. Several approaches were used to obtain high coercivity through magnetic grains isolation. Cr as underlayer causes to segregate the magnetic grains because of the columnar growth on the substrate [3]. Addition of non-magnetic atoms with large atomic volume to Cr (such as Mn [4], W [5], V [6] and Ti [7]) also increases the coercivity because it affects the lattice parameters of the underlayer. Addition of Pt to CoCr-based alloys decreases the inter-granular magnetostatic interaction, but excessive addition causes to increase it through increasing the stacking fault density and degrading the grain boundaries structure. Therefore, substitution of Pt by other elements is necessary. Niobium as a non-magnetic transition element substitutes in Co lattice and enlarges the lattice parameters. It also diffuses in grain boundaries and segregates the magnetic grains; thereby it causes reduction of the inter-granular magnetostatic interaction. The magnetic properties [8,9] of the films can be remarkably improved using the intermediate layer between the magnetic layer and underlayer. A proper thickness ratio of the two upper and intermediate magnetic layers provides the opportunity to investigate any effects of the grain nucleation behavior and the ready oxidation of Nb. The crystallographic matching between the crystal structure of Co alloy with Cr underlayer is said to be the main source to improve the magnetic properties of the magnetic layer separated by an intermediate layer [10]. In fact, intermediate layer induces a favorable orientation of the easy axis in the magnetic layer thereby enhances coercivity and magnetic squareness. Supplementary processes such as post-annealing improve magnetic properties of the films without any significant effect on the structure. In our previous work [11] the effect of post-annealing on the single-layer CoCrPtNb thin film was investigated. The results showed notable changes in magnetic properties and microstructure with sharp increase in coercivity of the annealed films.

[a] e-mail: almac@kashanu.ac.ir

The aim of the present work is to study the effect of post-annealing and thickness ratio of $(CoCrPt)_{97.5}Nb_{2.5}$/$Co_{75}Cr_{13}Pt_{12}$ (as upper and intermediate magnetic layers, respectively) on the magnetic properties and microstructure of $(CoCrPt)_{97.5}Nb_{2.5}/Co_{75}Cr_{13}Pt_{12}$ thin films deposited onto Cr underlayer. The magnetic effects were studied by hysteresis loops, switching field distribution curves and magnetic force microscopy images.

2 Experimental

Since the addition of Nb to as-depoisted CoCrPt causes the coercivity to decrease [12], then it seems that the addition of an intermediate magnetic layer improves the problem. The CoCrPtNb/CoCrPt/Cr layers were deposited onto Si (100) substrate without preheating using the DC magnetron sputtering technique at room temperature. At first, substrates were ultrasonically cleaned in acetone for about 30 min. The base pressure was 3×10^{-8} mbar. High-purity Ar (99.9999%) was used as sputtering gas at a pressure of 5×10^{-3} mbar. A 70 nm thick Cr underlayer was initially deposited on the substrate. The overall thickness of $(CoCrPt)_{97.5}Nb_{2.5}/Co_{75}Cr_{13}Pt_{12}$ layer was maintained at a constant thickness of 75 nm, while thickness of the upper magnetic layer ($(CoCrPt)_{97.5}Nb_{2.5}$) was 0, 15, 30, 45, 60 and 75 nm. The alloy films were co-deposited from the $Co_{75}Cr_{13}Pt_{12}$ and Nb targets. As reported in our previous work [12] addition of $\sim 2.5\%$ Nb slightly affected the remanence, squareness and magnetization taken from hysteresis loops. Annealing was performed at 600 °C for 15 min. The vacuum in the annealing furnace was 3×10^{-7} mbar with heating and cooling rates of $250\,^{\circ}\mathrm{C} \cdot \mathrm{min}^{-1}$.

Magnetic measurements were carried out by a Lake Shore 7300 vibrating sample magnetometer (VSM) system at room temperature. The microstructure information was obtained by X-ray diffraction (XRD) in θ–2θ mode, in which 2θ varied in the range of 35–55° with 0.05° interval (Philips X'pert, Cu K_α radiation source). A JEOL-200CX transmission electron microscopy (TEM) and an atomic force microscopy (AFM) were used to study the microstructure and morphology of the samples. The magnetic force microscopy (MFM) images were obtained by tapping mode of a digital instrument (DI), Nanoscope 3D controller Dimension 3100.

3 Results and discussion

3.1 Structural properties

Figure 1 shows XRD patterns of the as-deposited and annealed films as a function of the upper magnetic layer thickness. All the films show the Cr underlayer exhibited strong (110) texture overlapped with hcp-Co (002) maximum. In order to determine the exact position and intensity of the overlapped Co peak, deconvolution was performed. To clarify variation of the crystalline orientation of the samples, I_{100}/I_{101} and I_{100}/I_{002} ratios (as order parameters) are calculated and presented in figs. 1(c) and (d). In the as-deposited films, with increasing (decreasing) the upper magnetic (magnetic intermediate) layer thickness up to 30 nm (15 nm) *c*-axis rotates toward the film plane. After that with increasing the thickness to 45 nm (30 nm), it rotates toward the normal direction of the film plane. Through passing this critical thickness the crystalline orientation rotates close-to-plane orientation of (101) (see fig. 1(b)). Comparing these ratios for the as-deposited samples and randomly oriented Co film ($I_{100}/I_{101} = 0.2$, $I_{100}/I_{002} = 0.3$) (reported by Ono *et al.* [13]) shows a dominant out-of-plane and close-to-plane directions of the magnetic easy axis for the films with the upper magnetic layer thickness of 45 and 75 nm, respectively. Increasing intensity of the Co (101) peak (close to in-plane direction) in the annealed films comparing with the as-deposited ones is clearly observed. This result indicates improving of the crystalline orientation toward the film plane which expects to increase the coercivity. This orientation may generally result from the nearby in-plane atomic density of Cr underlayer and Co-based alloy [14]. Intensity ratio of the in-plane, close-to-plane and out-plane XRD peaks of the annealed samples also imply dominant orientation of (101) (see fig. 1(d)). The Scherrer equation [15] shows that, with an increase in the thickness of the upper magnetic layer from 0 to 45 nm in the as-deposited samples, the crystallite size of Co decreases from 21.28 nm to 10 nm. Further increase in the thickness increases the crystallite size to 15 nm. X-ray diffraction pattern investigations also show improving of the in-plane crystallographic texture of the annealed samples. Due to expansion of hcp-Co lattice through substitution of Nb in the unit cell of the alloy, hexagonal XRD maxima are slightly shifted to the lower angels. This will provide a better matching base between the magnetic layer and Cr underlayer. Therefore magnetic easy axis of the quaternary layer is more close to the plane of film than the ternary one.

The electron diffraction pattern of Cr underlayer (inset of fig. 2(a)) shows a bcc structure with (110) preferential crystalline direction, which is clarified by the XRD result. The bright field TEM image of Cr shows relatively uniform distribution of the grain size in the range of 20–25 nm. Diffraction pattern of the as-deposited film with upper magnetic layer thickness of 45 nm shows hcp crystal structure, in which *c*-axis oriented out- plane of the film (according to XRD pattern). The bright contrast regions in TEM images are related to mass/composition fluctuations and amorphous structure somewhat caused by addition of Nb [12].

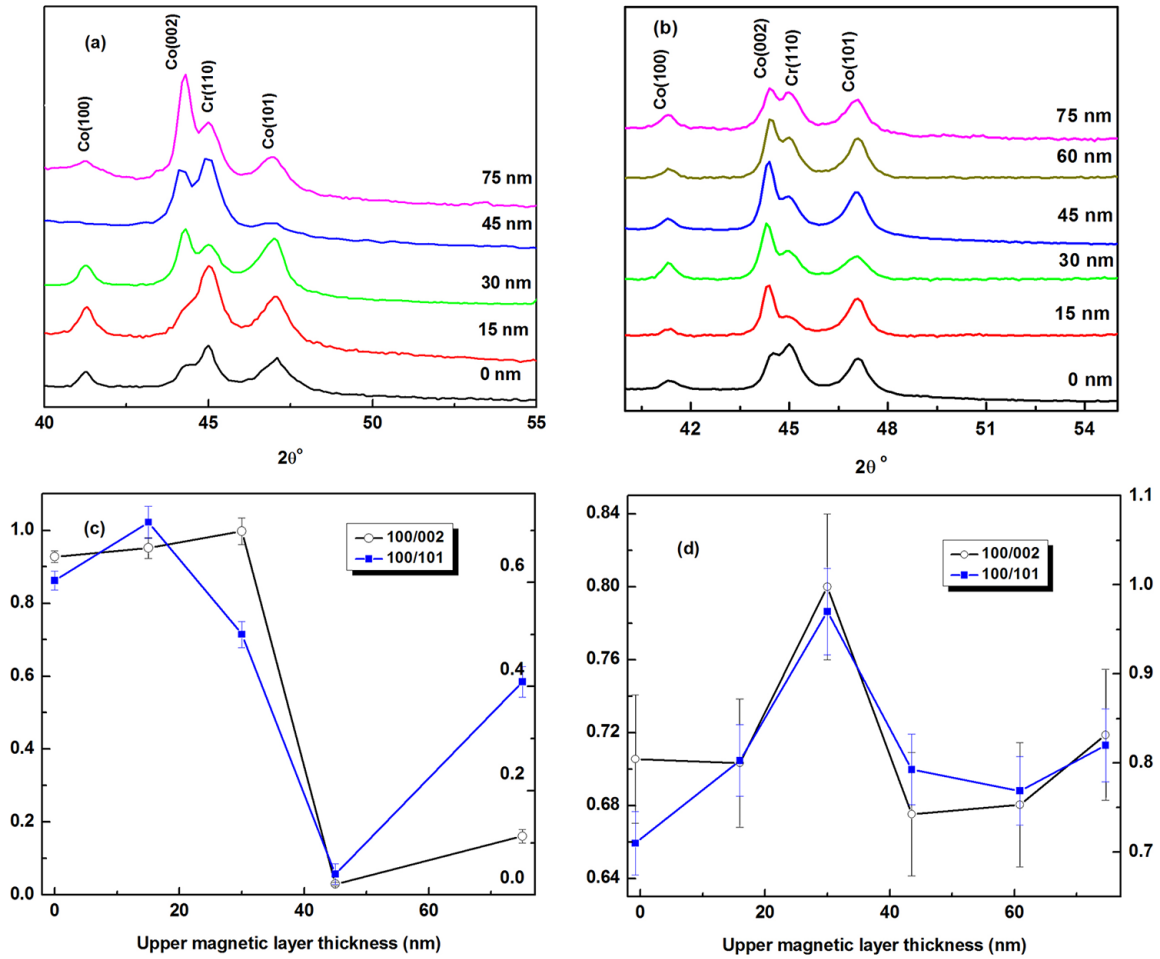

Fig. 1. XRD patterns of (a) as-deposited and (b) annealed films and ((c), (d)) intensity ratio of XRD peaks as a function of bilayer thickness ratio.

The comparison of TEM images of the as-deposited and annealed ternary films (figs. 2(b) and (d)) with the as-deposited and annealed films with 45 nm upper magnetic layer (figs. 2(c) and 2(e)) indicates an increase in the width of the amorphous channels and decreasing the number of the diffracting grains with dark contrast. Recrystallization of the amorphous structure and aggregation of the small grains during the annealing causes to form a non-uniform grain size distribution. However the average grain size is not considerably affected by annealing. Diffraction pattern of the annealed samples also shows a hexagonal close-packed structure, in which the c-axis orients slightly out plane of the film (in agreement with previously mentioned XRD results). Discontinuity of the diffraction ring of the annealed films also implies relatively larger grain size.

AFM images show reduction of root mean square (RMS) as indicator of the surface roughness of the as-deposited films from 2.174 to 1.741 nm, when upper layer thickness increases from 0 to 45 nm, while it increases to 1.952 nm for the quaternary configuration of the film. This roughness treatment arisen from Nb additive which forms amorphous channels between the magnetic grains (according to fig. 2(b)). It is previously reported [16–19] that columnar growth of the grains on the surface (based on the Thornton model [20]) is induced by Cr underlayer. It should be noted that surface roughness of the single-layer $Co_{75}Cr_{13}Pt_{12}$ is higher than single- and bi-layer $(CoCrPt)_{97.5}$ $Nb_{2.5}$ films. AFM images of the annealed films show the same roughness treatment; it initially decreases from 2.018 nm to 1.995 nm for 45 nm upper magnetic layer, then increases up to 2.128 nm for the quaternary film. It is observed that annealing has no significant effect on the roughness and roughness trend of the films as a function of increasing thickness of the upper magnetic layer. After annealing, the larger grain size with narrow distribution is obviously observed.

The lattice parameters (a, c) of the hexagonal close-packed structure and c/a ratio of all the as-deposited and annealed films are calculated and shown in table. 1. Small variation in the c, a parameters and their ratio is directly associated with increasing thickness of the layer containing Nb atoms. However, general reduction trend of the lattice parameters after annealing may be related to deplete the non-magnetic Nb from the CoCrPt lattice.

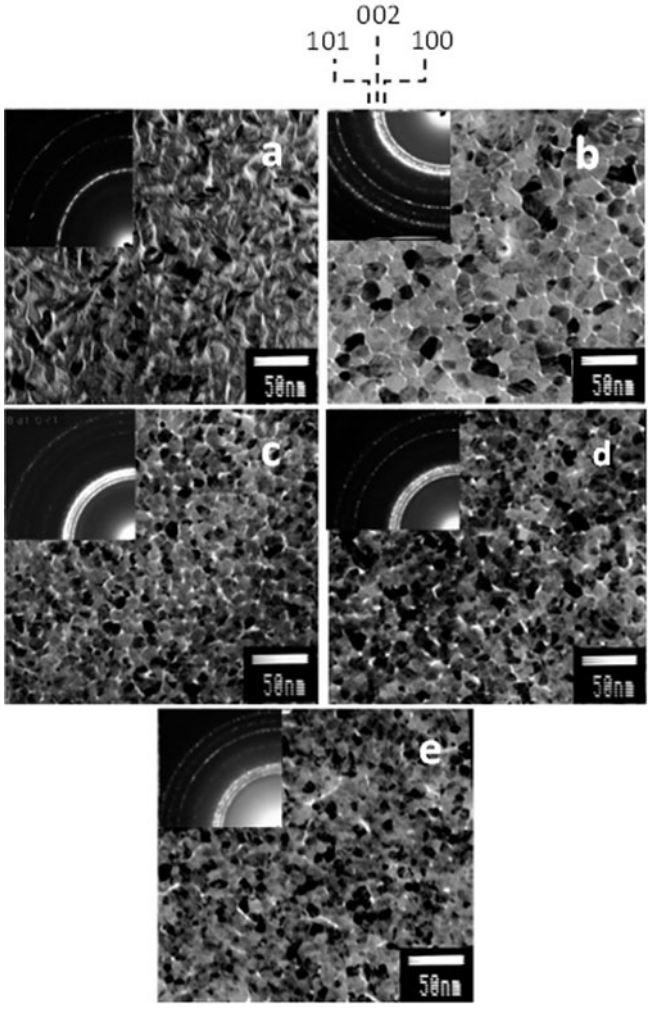

Fig. 2. TEM images of (a) Cr underlayer, as-deposited CoCrPtNb/CoCrPt/Cr film with upper magnetic layer thickness of (b) 0 and (c) 45 nm, annealed CoCrPtNb/CoCrPt/Cr film with upper magnetic layer thickness of (d) 0 and (d) 45 nm (diffraction patterns are presented in the inset).

Table 1. Lattice parameters for as-deposited and annealed samples (calculated from XRD patterns).

Upper magnetic layer thickness (nm)	c (nm)		a (nm)		c/a	
	As-deposited	Post-annealed	As-deposited	Post-annealed	As-deposited	Post-annealed
0	4.116	4.114	2.557	2.551	1.610	1.613
15	4.134	4.127	2.554	2.550	1.619	1.618
30	4.134	4.131	2.555	2.551	1.618	1.619
45	4.132	4.126	2.557	2.552	1.616	1.617
60	4.133	4.122	2.552	2.548	1.620	1.618
75	4.147	4.123	2.564	2.555	1.617	1.614

A possible explanation for the reduction trend of the c/a ratio for the annealed quaternary film is maybe the formation of the niobium oxide; in competition of heats formation of -1900, -900 and $-1100\,\mathrm{kj \cdot g \cdot mol^{-1}}$ for the oxides of Nb, Co and Cr, respectively [21]. It was reported [22] that addition/diffusion of Cr into the hexagonal lattice of the magnetic layer has no effect on the lattice parameters.

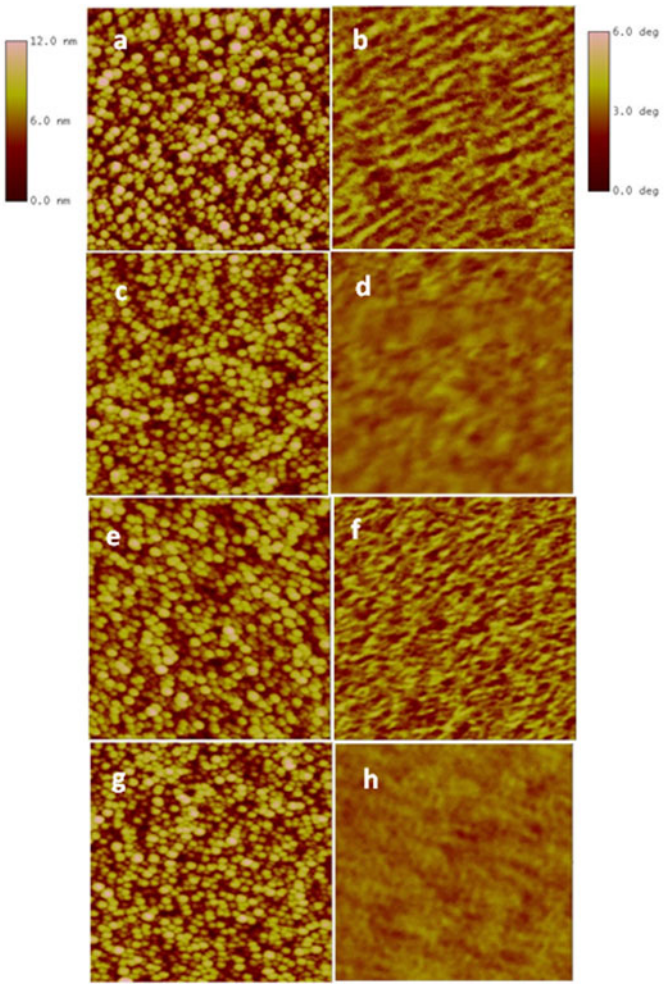

Fig. 3. AFM and MFM images of ((a), (b)) as-deposited, ((c), (d)) annealed CoCrPt/Cr film and ((e), (f)) as-deposited, ((g), (h)) annealed CoCrPtNb/Cr film.

3.2 Magnetic properties

MFM images of the as-deposited and annealed samples are also shown in fig. 3. The dark and bright contrasts present regions in which the magnetic moments are aligned in different directions. The change in magnetic layer composition of both the as-deposited and annealed films from ternary ($Co_{75}Cr_{13}Pt_{12}$) to the quaternary ($(CoCrPt)_{97.5}Nb_{2.5}$) reduces the image contrast, which means decreasing of the magnetostatic interaction. Since the images are random patterns, magnetic surface roughness can be used as an indicator of the contrast. Magnetic roughness of as-deposited (annealed) films decreases from 0.65° (0.4°) to 0.54° (0.3°) when the film composition varies from ternary to the quaternary ones. This trend shows a reduction in magnetostatic interaction of the films (see also fig. 4).

Figure 4 shows hysteresis loops of the as-deposited and annealed films when the external magnetic field is applied parallel to the film plane. The slope of switching region is inversely correlated to inter-granular coupling; more slope corresponds to a weaker coupling [23]. A possible origin of the inter-granular coupling could be segregation of magnetic grains by non-magnetic elements (See AFM and TEM images). The weakest coupling belongs to the film with 30 nm thickness of the upper magnetic layer which has the highest coercivity (see fig. 4(b)). The change in saturation magnetization (M_s) is attributed to distribution of small particles [15] and magnitude of Co as magnetic element in the layer. Due to the reduction of the magnetic atoms in the layer, the magnetization decreases when the thickness of the magnetic layer containing Nb atoms increases. As can be seen, the ternary layer has maximum magnetization while the quaternary film has the minimum one.

The obtained coercivities are plotted in fig. 4(c). As can be seen, it initially increases to a maximum of 1650 Oe for the 30 nm thick upper magnetic layer and then drops to 1300 Oe with increase in the thickness to 60 nm. Further increase in the thickness enhances coercivity up to 1580 Oe. Such a trend is previously seen in the order parameter, which clearly indicates correlation between the change in the magnetic easy axis and coercivity with increasing the intermediate magnetic layer.

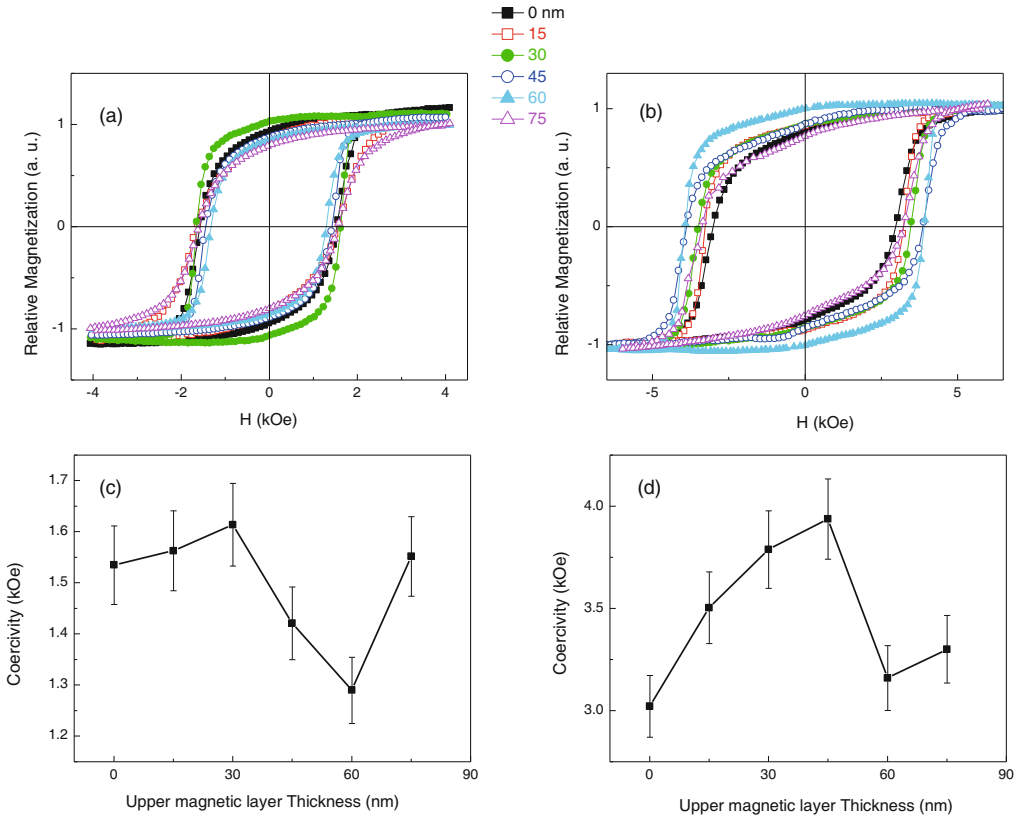

Fig. 4. In-plane hysteresis loops of (a) as-deposited, (b) annealed films and H_c variations of (c) as-deposited, (d) annealed films as a function of the thickness ratio.

Table 2. FWHM measured from SFD derived from DCD and IRM curves.

Upper magnetic layer thickness (nm)	0	45
$FWHM_{DCD}$	0.53	0.44
$FWHM_{IRM}$	0.79	0.63

Increasing the surface roughness reduces inter-granular interaction, while rotation of the *c*-axis towards the plane of film increases the coercivity. According to the crystalline orientation (obtained from XRD patterns) and surface roughness [24] (obtained from AFM images) of the samples, it seems that counterbalance between the two factors determines coercivity behavior. Variation of squareness of hysteresis loops with increasing the upper magnetic layer thickness also suggests variation of the inter-granular interaction. As can be seen, comparing with the annealed CoCrPt film, adding a layer containing Nb causes an increase in the magnetization. This may be related to sacrificial oxidation of Nb, which inhibits Co oxidation and, in turn, helps minimize any loss in the magnetization [16]. According to slope of the switching region, film with 30 nm upper magnetic layer has the weakest inter-granular coupling. Actually the coercivity of the samples significantly increases after annealing. It initially increases up to 3900 Oe for 45 nm upper magnetic layer thickness, then drops to 3150 Oe in the case of 60 nm thickness (see fig. 4(d)). The maximum coercivity of the annealed film with 45 nm upper magnetic layer may be attributed to a narrower distribution of the grain size (according to figs. 2(c) and (e)) and the *c*-axis oriented towards the film plane, while the higher coercivity of the annealed samples may be associated to Cr and/or Nb segregation, increase in pinning on demagnetization and also increase in the magneto-crystalline anisotropy in the Co-alloy grain [16]. Formation of the pure magnetic grains separated by Nb also causes coercivity to increase after annealing.

A measure of the inter-granular interaction is commonly obtained from switching field distribution (SFD) curves [14], which derived from a complete set of the normalized isothermal remanence magnetization (IRM) and DC demagnetization remanence (DCD) curves (see fig. 5). The width and intensity of the curves and adjustment of DCD and IRM maxima are a measure of inter-granular interactions. Full width half maximum (FWHM) of the both curves is calculated and presented in table 2. The results show increasing (decreasing) thickness of the upper magnetic layer (magnetic intermediate layer) up to 45 nm (30 nm) leads to increase in inter-granular interaction. However, further increase in the thickness reduces inter-granular coupling as a result of increasing the magnetic grains segregation (in agreement with AFM images).

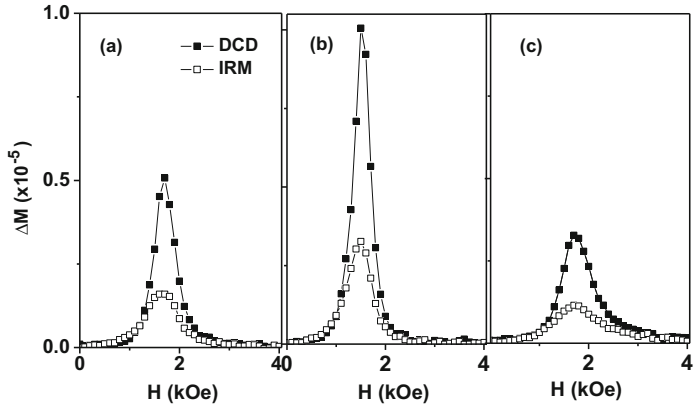

Fig. 5. SFD curves of as-deposited (a) ternary film, (b) film with upper magnetic layer thickness of 45 nm and (c) quaternary film.

4 Conclusions

Addition of intermediate CoCrPt layer up to 30 nm between Cr underlayer and CoCrPtNb layer improved magnetic properties through microstructure and texture improvement of the magnetic film. Annealing as a supplementary process through improving the in-plane crystalline texture of the films caused to enhance the coercivity. However, texture improvement alone could not modify magnetic properties. Another possible basic mechanism for the increasing coercivity of the annealed films is magnetic grain segregation.

Authors are grateful to the University of Kashan for supporting this work by Grant No (159023/2).

References

1. X. Yang, L. You, M. Song, G. Lin, Z. Li, Mater. Design **27**, 223 (2006).
2. X.F. Hu, Q. Liang, H.Q. Li, X.X. He, Xiaoru Wang, W. Zhang, Appl. Surf. Sci. **252**, 4625 (2006).
3. A. Kharmouche, S.M. Chérif, Y. Roussigné, G. Schmerber, Appl. Surf. Sci. **255**, 6173 (2009).
4. M.A. Parker, J.K. Howard, R. Ahlert, K.R. Coffey, J. Appl. Phys. **73**, 5560 (1994).
5. L.S. Tian, L. Xi, S.W. Kui, C.J. Wei, W.F. Lin, W. Dan, Chin. Phys. B **18**, 1643 (2009).
6. S.S. Malhorta, D.C. Strafford, B.B. Lal, C. Gao, M.A. Russak, J. Appl. Phys. **85**, 6157 (1999).
7. T.D. Lee, M.S. Hwang, K.J. Lee, J. Magn. Magn. Mater. **235**, 297 (2001).
8. H.S. Lee, D.E. Laughlin, J. Appl. Phys. **91**, 7065 (2002).
9. P. Glijer, J.M. Sivertsen, J.H. Judy, J. Magn. Magn. Mater. **140**, 2219 (1995).
10. S. Park, D.E. Laughlin, J.G. Zhu, IEEE. Trans. Magn. **46**, 2278 (2010).
11. M. Almasi-Kashi, S.P.H. Marashi, R. Pouladi, P.J. Grundy, Thin Solid Films **518**, 2157 (2010).
12. K. Ono, B. Wong, J. Appl. Phys. **68**, 4734 (1990).
13. P. Scherrer, Gött. Nachrich. Gesell. **2**, 98 (1918).
14. M. Almasi-Kashi, P.J. Grundy, G.A. Jones, H. Nadgaran, X. Zhao, J. Magn. Magn. Mater. **248**, 190 (2002).
15. Y. Okumura, O. Suzuki, H. Morita, X.B. Yang, H. Fujimori, J. Magn. Magn. Mater. **146**, 5 (1995).
16. Y. Liu, B.W. Robertson, Z.S. Shin, S.H. Liou, D.J. Sellmyer, J. Appl. Phys. **77**, 3831 (1995).
17. J. Han, M. Hintz, J. Sexton, J. Skorjanec, G. Lundstrom, Thin Solid Films **518**, 2179 (2010).
18. S.H. Lee, Curr. Appl. Phys. **12**, 93 (2012).
19. J.A. Thornton, J. Vac. Sci. Technol. **12**, 830 (1975).
20. O. Henkel, Phys. Status. Solidi B **7**, 919 (1964).
21. E.P. Wohlfarth, J. Appl. Phys. **29**, 595 (1958).
22. M.L. Plumer, J.V. Ek, D. Weller, *The physics of ultra-high density magnetic recording*, 4th edition (Springer, New York, 2001).
23. B.J. Boyle, E.G. King, K.C. Conway, J. Am. Chem. Soc. **76**, 3835 (1954).
24. K. Kobayashi, G. Ishida, J. Appl. Phys. **52**, 2453 (1981).